Available online at www.sciencedirect.com
SCIENCE DIRECT®
PERGAMON
International Journal of Heat and Mass Transfer 46 (2003) 1279–1292
International Journal of HEAT and MASS TRANSFER
www.elsevier.com/locate/ijhmt

Investigation of the evaporation of embedded liquid droplets from porous surfaces using magnetic resonance imaging

N.C. Reis Jr. [a,*], R.F. Griffiths [b], M.D. Mantle [c], L.F. Gladden [c]

[a] Dept. de Informática, CT-UFES, Av. Fernando Ferrari, S/N, CEP 29060-970 Vitória, ES Brazil
[b] Environmental Technology Centre, Department of Chemical Engineering, UMIST, P.O. Box 88, M60 1QD, UK
[c] Department of Chemical Engineering, University of Cambridge, Pembroke Street, Cambridge CB2 3RA, UK

Received 11 December 2001

Abstract

For the first time, results are presented from studies using magnetic resonance imaging techniques to follow the behaviour of single water droplets evaporating from porous surfaces. The droplets are initially embedded in the porous substrate by impingement, and are then evaporated over a period of several hours, the surface of the substrate being ventilated by a controlled airflow. The configuration is intended to mimic the behaviour of droplets evaporating into atmospheric flows from surfaces such as sand, or concrete. The method produces several types of data, including images of impinged droplets inside the porous substrate and their development with time during the evaporation episode, one-dimensional concentration profiles through the substrates, and corresponding estimates of the mass fraction of liquid remaining, evaporation rate and mass flux per unit area. The results obtained show that the impinged droplet resides in the porous medium in a shape similar to a semi-spheroid. The results also indicate that the transport of liquid by capillary diffusion has a very strong influence upon the evaporation process, providing a challenge to the simple receding evaporation-front assumption that is utilised in many modelling procedures.

1. Introduction

The study of the impact and evaporation of liquid droplets on porous surfaces is important for a wide range of situations, varying from environmental applications to inkjet printing technology. When a liquid droplet impinges on a permeable flat surface, there is a rapid increase in the pressure at the impact region, transforming the axial momentum of the liquid into a radial fluid flow. At the same time the pressure at the impact point also forces the liquid to move through the permeable surface. If the resistance imposed by the porous substrate is large enough to prevent complete liquid absorption, part of the liquid may reside as a lens-shaped mass over the surface of the substrate, while the rest of liquid is embedded in the porous substrate. On the other hand, if the resistance imposed is not large enough, the liquid will be completely absorbed by the porous substrate. In either case the evaporation rate of the liquid droplet is considerably affected, since the process is dependent not only on the air stream over the droplet, but also on the transport mechanisms and phase change behaviour occurring inside the porous substrate.

Previous studies on this topic were mainly based on observations of the time evolution of the shape of the liquid droplet outside or on the surface of the porous substrate, during the impingement and/or the subsequent evaporation [2–5]. These studies reported detailed investigations conducted in laboratory, wind-tunnel and field experiments. However, there is still very little information about the shape of the liquid droplet and the behaviour of the liquid inside the porous medium. Further information is necessary to evaluate the

* Corresponding author. Tel.: +55-27-3335-2133; fax: +55-27-3335-2679.
E-mail address: neyval@inf.ufes.br (N.C. Reis Jr.).

0017-9310/03/$ - see front matter © 2002 Published by Elsevier Science Ltd.
PII: S0017-9310(02)00395-2

Nomenclature

A	area (m^2)
c	integrated concentration along the horizontal plane (kg/m)
dM/dT	evaporation rate (kg/s)
F	mass flux to the air stream ($kg/s\,m^2$)
M	mass of the liquid (kg)
r	droplet radius (m)
T	time (s)
v_r	vapour transfer velocity to the air stream (m/s)

Subscript

0	reference value

Superscript

$*$	non-dimensional value

importance of liquid transport during the evaporation episode to substantiate and validate model development. For instance, such information would clarify the validity of the assumption of the receding evaporation-front approach (assumed in some droplet evaporation models [1,2]), as well as the importance of a two or three-dimensional representation of the phenomenon.

Accordingly, the aim of this work is to provide information about the behaviour inside the porous medium. In order to achieve this objective, a magnetic resonance imaging (MRI) study was carried out to provide images of the shape of droplets inside the porous medium after the impact and throughout the evaporation episode. The experimental apparatus attempts to mimic to some extent the conditions applying to the evaporation of droplets exposed to the atmosphere, simulated by a controlled air stream on the surface of the porous substrate. It should be noted that the MRI apparatus very severely constrains the extent to which such a situation represents real atmospheric conditions.

2. Experimental set-up and procedure

The objective of the experimental work was to study the shape of the liquid droplet after the impingement, and to follow the variation of this shape as the droplet evaporates from within the porous medium, under conditions similar to those in the atmosphere. Accordingly, the experimental procedure described here tries to mimic atmospheric conditions inside the MRI magnet, where the evaporation process can be monitored and imaged. The droplet is delivered to a porous substrate inside the MRI magnet, and a carefully adjusted airflow is established over the porous surface, in order to ventilate the surface and support an evaporative mass flux similar to that in the atmosphere. In order to evaluate the influence of the porous medium itself, several porous substrates were tested.

2.1. Experimental set-up

All MRI acquisitions were performed using a Bruker DMX-300 spectrometer operating at a ^1H (proton) frequency of 300.13 MHz corresponding to a static magnetic field strength of 7.07 T. All one-dimensional profiles and two-dimensional images were acquired using a 15 mm diameter birdcage radiofrequency resonator. These dimensions restrict the maximum sample holder/set-up diameter to 14 mm. Spatial resolution was achieved using three-orthogonal axis (x, y and z) actively shielded gradient system capable of producing a maximum gradient strength of 1 T/m in all three cartesian directions. An experimental cell was built to provide the required ventilation airflow within this limited space. The ventilation cell consists of a Perspex tube and a flange, containing three internal orifices: one to supply the inlet airflow, another to allow the outlet airflow and a third used to place a capillary tube close to the porous surface and deliver the droplet (Fig. 1a).

The experimental procedure involves partially filling a test tube with a porous material (e.g. sand or glass beads), in order to obtain a well-defined porous layer (Fig. 1b). The ventilation cell is then carefully lowered down the bore of the magnet so that it forms a lid close to the surface of the porous substrate. A capillary tube (connected to a syringe pump) was used to deliver a liquid droplet to the porous substrate. Rapid in situ on line one-dimensional profiling was used to monitor the progress of a single droplet starting with the formation of the droplet at the capillary orifice to its impingement on the porous substrate. After the droplet had been delivered to the substrate an airflow was maintained via the inlet and outlet orifices, creating an airflow parallel to the porous surface.

2.1.1. Determination of the flow rate of the air supply

In order to simulate evaporation under atmospheric conditions the air supply must be carefully controlled. However, it is not possible to simulate the turbulence levels and the pattern of the airflow in the atmosphere inside such a small apparatus. Nonetheless, it can be argued that this is not a serious deficiency, since the crucial factor is the magnitude of the evaporative mass flux through the surface of the porous medium. If the flow velocity inside the cell is carefully adjusted, it is possible to approximately match the mass flux expected

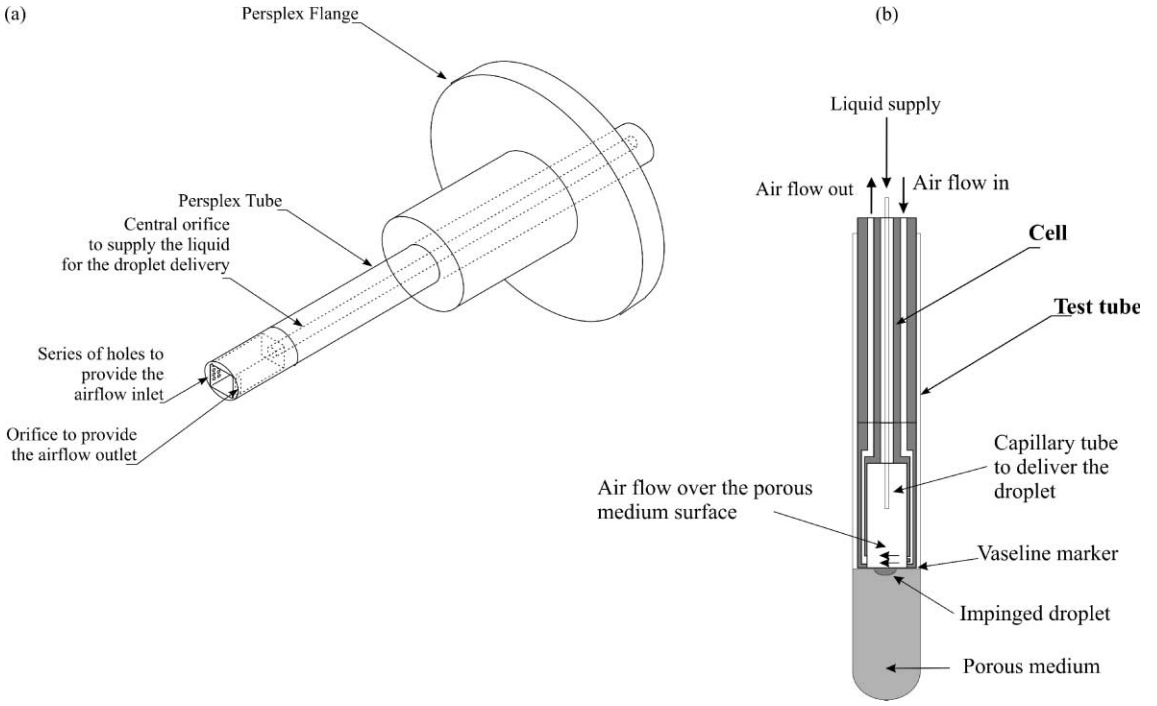

Fig. 1. (a) Perspective view of the Perspex cell. (b) Detailed view of a longitudinal section of the cell placed inside the test tube containing the porous substrate.

under given atmospheric conditions and the mass flux obtained in the cell. If this matching is achieved, the phenomena displayed within the porous medium in the NMR experiment should be representative of those occurring in a field situation.

The mass flux to the air stream is usually parameterised as [1]:

$$F = v_r(c_s - c_r) \tag{1}$$

where F denotes the mass flux to the air stream (kg/m^2 s), v_r is the mass transfer coefficient (m/s), c_s is the vapour concentration at the surface (kg/m^3) and c_r is the vapour concentration (kg/m^3) in the air stream. The value of c_r is usually taken to be equal to zero, as the background concentration is often neglected [2,6]. The value of v_r is mainly dependent on the characteristics of the airflow (especially the friction velocity).

By using this parameterisation, the mass flux to the air stream can be treated as a convective transport of vapour, with characteristic velocity v_r determined by the transport mechanisms through the air stream/porous surface interface. For droplets evaporating exposed to atmospheric flows, the value of v_r ranges from 0.02 to 0.15 m/s, depending on the wind velocity and turbulence conditions (these values are based on expressions presented in [1]). In order to determine the value of v_r inside the cell, and thereby to simulate evaporation of droplets exposed to the atmosphere, a computational fluid dynamics (CFD) model of the fluid flow inside the cell was developed. In order to validate this procedure, the mass flux values obtained during the experiments were compared with field experimental data reported in [7], and a relatively good agreement was found, the CFD simulation values being within 10–15% of the corresponding field data. [1]

2.2. Experimental procedure

In this study two-dimensional and one-dimensional imaging techniques are used. While the two-dimensional images give qualitative information about the droplet shape after impingement and its variation throughout the evaporation episode, the one-dimensional images also yield quantitative information about the concentration profiles along the depth direction in the porous substrate. The concentration profiles are then used to determine the mass fraction of liquid remaining in the substrate, and the corresponding values of evaporation rate and mass flux to the air stream.

Each MRI acquisition cycle comprises a one-dimensional water droplet profile acquisition and a two-dimensional slice selective water droplet image

[1] The data involved in these comparisons are not presented here because of space limitations. For a full description see [8].

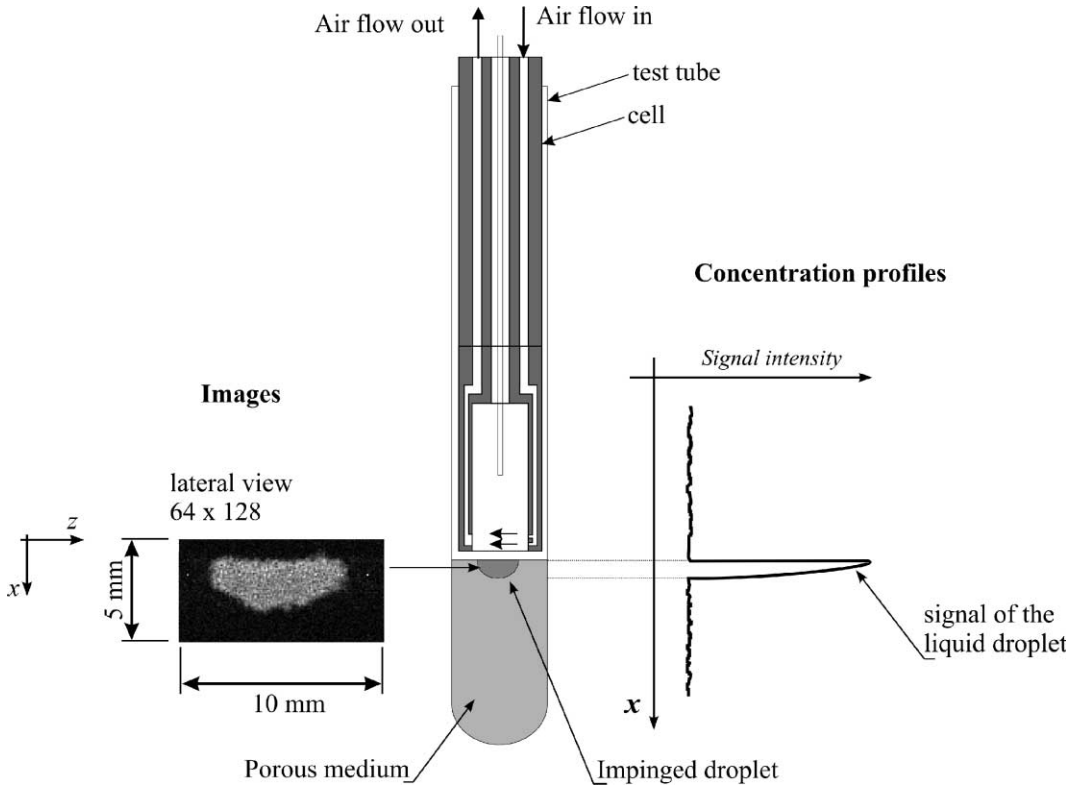

Fig. 2. General representation of a lateral (*xz*-slice) two-dimensional image of the liquid droplet just after impingement and a corresponding water concentration profile.

acquisition. During the full evaporation episode many such acquisition cycles are performed, generating a time series of images that is used to reconstruct the time evolution of the drying phenomenon. Fig. 2 shows schematic representations of the two-dimensional image and the corresponding concentration profiles. The following sections present a short description of these experimental procedures.

2.2.1. Two-dimensional images

The entire evaporation episode for a single drop typically takes about 2–4 h, depending on the flow rate of the ventilation air supply and the properties of the liquid. In order to obtain the time evolution of the shape of the droplet, several lateral (*xz*-slice) view images of the droplet were taken during the evaporation episode, at intervals of approximately 5 min.

Two-dimensional slice selective proton spin-echo images of water droplets were acquired using a fast spin-echo RARE pulse sequence [9]. One hundred and twenty eight points were sampled in the gradient frequency encoding (*z*) direction and 64 phase encoding (*x*) gradients were used yielding a final image of 128×64 pixels. All 2D proton images were acquired with a field of view of 10 mm in the radial direction and 5 mm in the axial direction corresponding to an isotropic spatial pixel resolution in the *xz*-plane of 78 μm. The slice thickness in the *xz*-plane was 1.5 mm. A 'RARE' factor equal to 4, and eight accumulations, at a recycle time of 1.5 were used to obtain each two-dimensional image giving a total imaging acquisition time equal to 3.2 min. A RARE factor of 4 was chosen as a reasonable compromise between image acquisition speed and image quality.

As neither the Perspex cell nor the porous substrate (glass beads or sand) have a detectable NMR signal, the images obtained display only the shape of the liquid droplet, and the brightness of each pixel indicates the concentration of liquid at the corresponding position.

2.2.2. One-dimensional images or profiles

One-dimensional proton profiles of water droplets were acquired using a standard spin-echo profiling image sequence with an echo time, $TE = 2.54$ ms, a recycle time, $TR = 6.0$ s and eight averages were acquired. The total acquisition time was approximately 1 min. A field of view of 20.0 mm was used and 256 data points were acquired giving a digital one-dimensional spatial resolution of 78 μm [10].

This procedure gives the profile of liquid concentration with depth in the substrate (along the *x*-axis in

Fig. 2), where the signal at each position is proportional to the integrated concentration along a horizontal plane of the impinged droplet. As the acquisition time (1 min) is not very long in comparison with the total evaporation time of a sample, we believe that there is negligible drying during the acquisition of the profile data.

Since the amount of liquid delivered to the porous substrate is known, it is possible to correlate (normalise) the total intensity of the signal obtained by one-dimensional profiling, i.e. the integral of the signal along the entire thickness of the porous medium, with the known mass of the liquid droplet. Thus, it is possible to translate the signal intensity into liquid concentration units, and express the profile graphs (Fig. 2) as integrated concentration [2] (kg/m) vs. x (m). In addition, the rate of change of the signal integrated over the entire thickness of the porous medium can provide the evaporation rate of the liquid droplet, since the total signal is proportional to the mass of liquid present in the substrate.

2.3. Accuracy considerations

Although the intensity of the signal obtained from each scan is proportional to the concentration of liquid at each point of the sample, it is necessary to account for the signal loss due to relaxation. Quantitative results from MRI may only be obtained when a full detailed knowledge of the spin–lattice (T_1) and spin–spin (T_2) relaxation time constants of the system under study are known. A detailed discussion of how T_1 and T_2 relaxation times affect image quantitation is beyond the scope of this text and the reader is referred to the monograph by Callaghan [10].

Bulk, i.e. non-spatially resolved T_2 measurements were carried out for single drop of water impinged on the 180 μm sand, 50 μm glass beads and 120 μm glass beads using a Carr–Purcell–Meiboom–Gill spin-echo magnetic resonance method [11]. In the initial stages of the experiments the T_2 average value is approximately 126 ms (T_2 50 μm beads = 120 ms; T_2 120 μm beads = 125 ms; T_2 180 μm sand = 133 ms) which makes the amount of signal lost due to T_2 relaxation practically negligible (less than 2.0%) for one-dimensional profile experiments. For RARE image acquisition, since an echo time of 12.64 ms [3] was used, the loss of signal in the initial stages is approximately 9.5%. However, as the evaporation proceeds the amount of liquid in the sample is reduced and the value of T_2 value decreases as the amount of 'free' liquid changes [10]. In the final stages of the evaporation process the average T_2 value (T_2 50 μm beads = 34 ms; T_2 120 μm beads = 30 ms; T_2 180 μm sand = 30 ms) is approximately equal to 31 ms, which represents a signal loss of approximately 33% for the images and 7.9% for the profiles.

The bulk T_1 value for the all systems was found to be between 1.6 and 2.0 s (for 50 and 400 μm glass beads, respectively). This implies that a maximum of only 5% of the available water signal is lost due to T_1 relaxation, as the recycle time of our profile experiments was 6.0 s.

Therefore, when analysing the time evolution of the concentration profiles inside the porous medium, one must bear in mind that there is a small, but significant, influence of the signal degradation due to T_1 and T_2 relaxation (approximately 7% of signal loss at the beginning, and 12% at the end of the experiments, for concentration profiles). This will have two main effects: (i) the rate of loss of signal is slightly higher than the evaporation rate of the droplet, since the rate of signal loss includes the evaporation rate plus an decrease in the value of the T_2 relaxation time towards the end of the experiments; (ii) there is a minimum concentration detectable; very small liquid concentrations will present a smaller T_2 relaxation time reducing even more the amount of signal recorded.

In order to determine the minimum concentration detectable, the samples were weighed before the droplet delivery (i.e. only the test tube + porous substrate) and after the drying, so that if there was any residual liquid undetected after the drying, it would show up as an increase in weight of the sample. The measurements indicate an average residual mass of 0.9 ± 0.6 μg, which is equivalent to 4.69% of the initial mass of the droplet. This indicates a probable residual concentration of approximately 11.43 ± 8.33 kg/m^3, which was determined using the approximate volume of the impinged droplet obtained from the NMR images.

This value represents the undetectable (by MRI profiling) moisture in the sample for the concentration profile scans. For the two-dimensional images, the minimum concentration of detectable water is higher, and therefore the water signal from the images disappears well before that of the profiles. By comparing the profile data and the images, it is possible to estimate that concentrations smaller than 28.59 ± 5.27 kg/m^3 are not detected on the 2D images. [4]

[2] Integrated concentration is defined as liquid concentration in the porous medium integrated over the area of the horizontal plane.

[3] This value is calculated considering a RARE imaging sequence with four echoes, spaced by 3.16 ms, i.e. it is necessary to account for the signal degradation of each echo and the summation of the signal of the four echoes.

[4] Value determined by using the approximate volume of the impinged droplet obtained from the NMR images just after impingement and the total signal recorded by the profiles for the time interval that there is no longer signal recorded by 2D images.

Compared with the liquid concentration inside the fully saturated region (approximately 500 kg/m^3), this amount is very small (2.79% for profiles). However, this does show that the use of NMR imaging to study the transport of liquid in non-saturated regions has some limitations. Nevertheless, the data provided by the concentration profile scans complements the data contained in the images.

2.4. Parameterisation

By normalising the data obtained using characteristic values for the evaporation of a free liquid surface exposed to a similar air stream, it is possible to analyse the limiting influence of the transport inside the porous medium upon the evaporation process. Accordingly, a characteristic mass flux can be estimated as (for a negligible background vapour concentration in the air stream):

$$F_0 = v_{r0} c_{sv} \tag{2}$$

where v_{r0} denotes the characteristic vapour transport velocity for a given flow rate and c_{sv} represents the value of the saturated vapour concentration in air. In order to determine the characteristic time scale, it is necessary to determine a characteristic area through which the flux F_0 transports the mass of the liquid droplet (M_0). A satisfactory magnitude for this area can be calculated by using the droplet radius prior to the impingement (r_0), since the radius of the wet spot after the impingement will be larger than r_0, but of the same order of magnitude. Therefore, the time scale of the process is defined as:

$$T_0 = \frac{M_0}{F_0 A_0} \tag{3}$$

where A_0 denotes the characteristic area ($A_0 = \pi r_0^2$).

This time scale represents the approximate time that an equivalent mass of liquid would take to evaporate from a fully saturated wet spot (i.e. a free liquid surface) with a radius equal to r_0, when exposed to the given air flow. Normalising the relevant variables of the problem by using characteristic time scale (T_0), mass (M_0) and mass flux (F_0), the following dimensionless parameters were introduced:

$$T^* = \frac{T}{T_0} \quad M^* = \frac{M}{M_0} \quad F^* = \frac{F}{F_0}$$

$$(\mathrm{d}M/\mathrm{d}T)^* = \frac{\mathrm{d}M/\mathrm{d}T}{F_0 A_0} \tag{4}$$

where T^* is the non-dimensional time, M^* is non-dimensional mass, also called mass fraction remaining, and F^* and $(\mathrm{d}M/\mathrm{d}T)^*$ are the dimensionless mass flux and evaporation rate.

By analogy with this treatment of time, mass flux, evaporation rate and droplet radius, it is also necessary to present the concentration profiles in non-dimensional form. As discussed previously, the concentration profiles of liquid inside the porous substrate are expressed in kg/m. Accordingly, it is necessary to specify a means of correlating the values in kg/m with the actual saturated liquid concentration for the porous medium.

The concentration profiles are expressed in kg/m because they represent the integrated concentration in the horizontal plane of the impinged droplet. In the same way, one can translate the actual liquid saturation concentration for the porous medium to kg/m by using the characteristic area of the impinged droplet (A_0). Thus, it is possible to rewrite the concentration of liquid as:

$$c^* = \frac{c}{c_0} \tag{5}$$

where c is the concentration expressed in kg/m and c_0 is the characteristic concentration ($c_0 = c_{\mathrm{sat}} A_0$), where c_{sat} is the saturated liquid concentration for the porous medium.

3. Results and discussion

The results presented here are divided into two main sections. In the first section, a basic configuration representing a typical droplet impingement/evaporation case is simulated, and the main features of the process are discussed. As a base configuration a water droplet (1.6 mm radius) was delivered to a porous substrate composed of 120 μm diameter glass beads, with an impact velocity of 0.5 m/s. The impinged spot was then exposed to a 10 ml/min air stream (v_r equal to 0.008 m/s, which is approximately equivalent to a friction velocity in the atmosphere of 0.1 m/s). In the second section, the same droplet configuration is tested on several different porous substrates.

3.1. Base case—outline of the physical mechanisms

For analysis purposes, it is possible to consider the phenomenon of droplet impingement/evaporation as two separate events, since several orders of magnitude separate the time scales of the mechanisms involved. The time scale of the droplet impingement/absorption is of the order of milliseconds. On the other hand, the time scale of the liquid motion due to capillary effects is of the order of minutes, [5] and the time scale of the evaporation

[5] This value is calculated based on the capillary diffusion coefficient value for sand [12] and the characteristic dimensions of the impinged droplet.

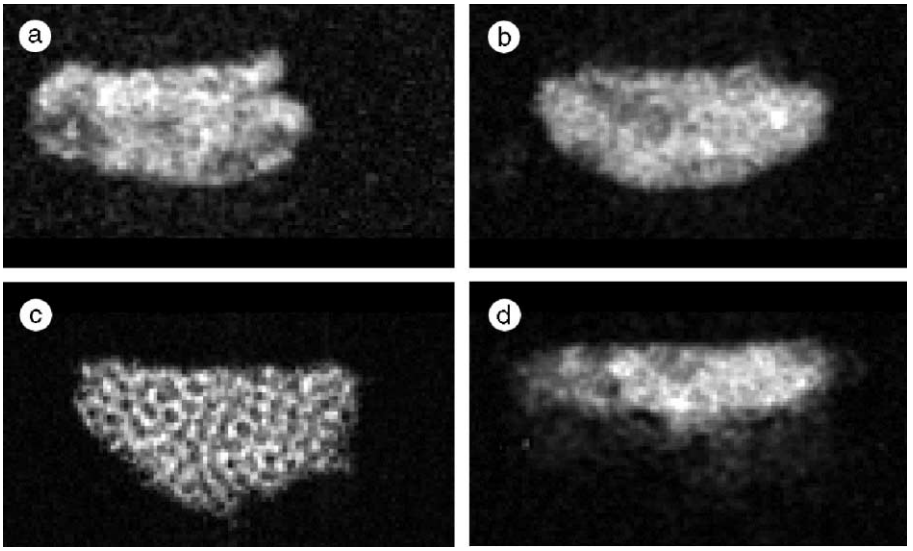

Fig. 3. *xz*-slice of the liquid droplet just after impingement, for (a) 50 μm glass beads, (b) 120 μm glass beads, (c) 400 μm glass beads and (d) 180 μm sand.

process for a liquid such as water is of the order of hours. Accordingly, the analysis presented here is performed in two separate steps. In the first step, the shape of the impinged droplet is analysed. In the second step, the evaporation process is analysed, where the shape of the impinged droplet is taken as the initial condition of the drying process.

3.1.1. Shape of the impinged droplet

When a liquid droplet impinges on a flat solid non-permeable surface, there is a rapid increase in the pressure at the impact region, transforming the axial momentum of the liquid in a radial fluid flow, which causes the droplet to spread over the surface. The problem of droplet impingement on permeable surfaces presents more complicated physical phenomenon, since at the same time that the axial momentum of the droplet is transformed to radial momentum, the pressure at the impact point also forces the liquid to move through the permeable surface. Furthermore, capillary effects draw the liquid into the porous substrate. As a consequence of this balance between lateral spreading and liquid penetration, the impinged droplet resides in the porous medium in a shape similar to a semi-spheroid, whose aspect ratio will depend on the porous medium and liquid droplet characteristics. Fig. 3b presents the first image obtained of the impinged droplet, just after the impingement.

There was a delay of approximately 1 min after initial impingement to the start of two-dimensional image acquisition. In addition, the total imaging time is approximately 5 min. Therefore, this image represents an integrated view of the impinged droplet over this period of time, and any variation in its shape during this period is not resolved.

The fairly definite shape shown in Fig. 3b indicates that the droplet exists as a fully saturated region with a relatively sharp interface. The position of the surface of the substrate is clearly distinguishable as the flat region on the upper side of the droplet. It should be noted that the upper surface of the droplet is not completely flat. These irregularities are caused by disturbances of the glass beads due to the impact with the liquid droplet, forming a small crater on the surface of the substrate.

The radius of the region occupied by the impinged droplet is $1.72r_0$ and the penetration depth is $1.10r_0$ It is evident that the liquid concentration is not uniform over the entire section of the droplet, since several shades of grey are present. The differences in concentration can be attributed to slight inhomogeneities in the porous medium packing. This fact will be more apparent in the analyses of the drying of the porous substrate performed in the next section.

There are also some lighter regions in some of the images, even outside the region occupied by the liquid droplet. These bright spots are not related to a liquid concentration, but appear to be artefacts of the image acquisition technique. These artefacts can be more clearly seen in the time series of images of the evaporation shown in the next section; even where the porous medium is completely dry, these parts of the image still show some intensity above the background noise level.

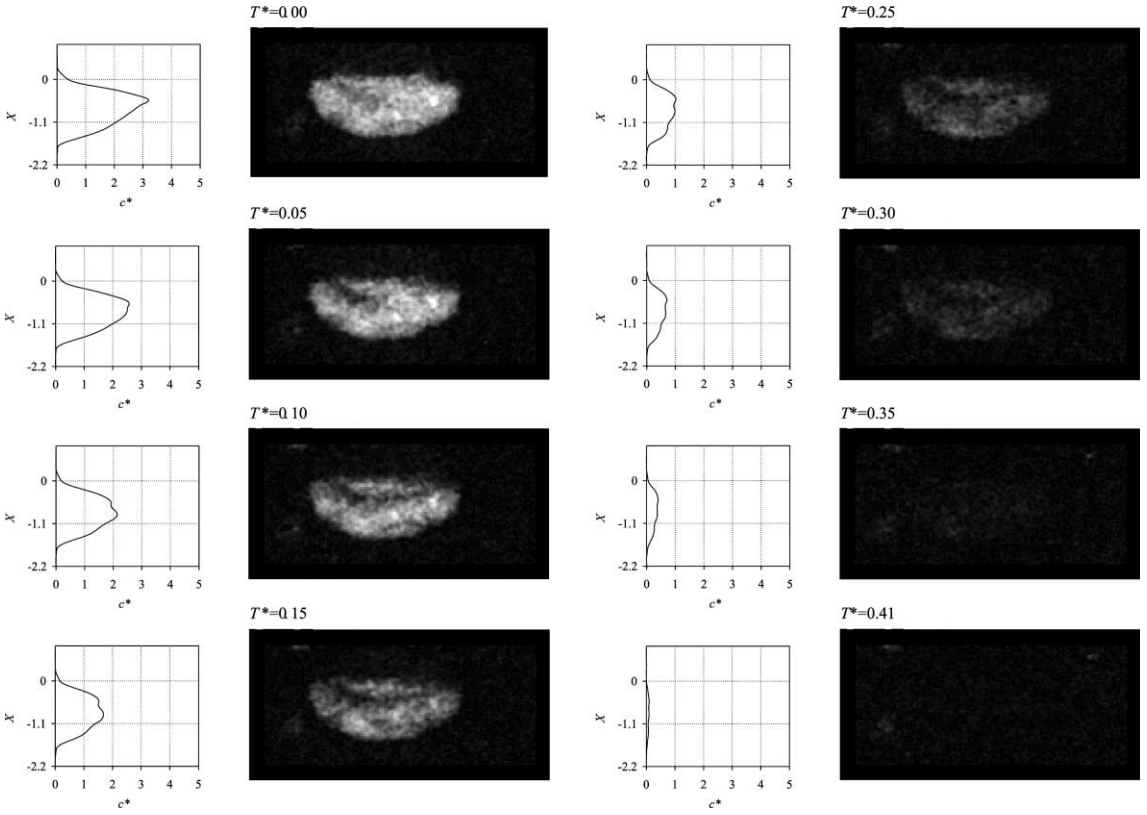

Fig. 4. Time evolution of the concentration profiles of liquid and images of the shape of the droplet inside the porous substrate for 120 μm glass beads.

3.1.2. Droplet evaporation

Fig. 4 presents the time evolution of the axial (z) concentration profiles of liquid, and the corresponding images of the shape of the droplet inside the porous substrate. It is important to inspect the two-dimensional images together with the one-dimensional concentration profiles, since the images provide information about the shape of the droplet, but only give limited quantitative information about the concentration of liquid inside the substrate. The profiles provide the complementary information concerning the concentration levels.

The first image presented in Fig. 4 is identical to that shown in Fig. 3b. It should be noted that there is a delay of approximately 1 min between an image and a profile, which is equivalent to $T^* = 0.003$. This time delay is negligible in comparison with the total duration of the evaporation episode $T^* \approx 0.5$ (≈150 min).

The profiles indicate a maximum concentration level very close to the substrate surface (region of maximum diameter of the impinged droplet). This value of c^* (slightly over 3) indicates that there is approximately three times more liquid mass in this region than there would be if there was a fully saturated region of liquid with radius equal to r_0 This result is physically sound, since the radius of the impinged droplet in this region is approximately $1.72r_0$ so that the area of the wet spot in the surface of the substrate is three times larger than that of a free liquid surface of radius r_0.

It also possible to observe small values of concentration in the region just above the nominal surface of the porous substrate ($x^* = 0$). This is related to the irregularities in the substrate surface after the droplet impingement. Inside the substrate the concentration levels in the profiles tend to zero approximately at the same depth as the image indicates the lower surface of the impinged droplet. The minimum concentration detectable in the images does not coincide with the minimum concentration detectable in the profiles, the latter being more sensitive. The fact that the profiles tend to zero at approximately the same depth as the image indicates a fairly definite droplet shape, with a sharp concentration gradient.

As the droplet evaporation proceeds, drying starts from the upper surface of the droplet, as can be clearly

observed by the reduction in the concentration levels of the profiles in the region close to the surface. This reduction in the concentration levels gradually changes the shape of the curve, so that at $T^* = 0.10$ the maximum concentration value is no longer close to the surface. This behaviour is more difficult to deduce from the images, and although it is possible to observe the general tendency of drying from the surface in the initial images ($T^* = 0.00$, 0.05 and 0.10), the drying process does not advance homogeneously through the liquid region. This behaviour can be mainly attributed to inhomogeneities in the porous medium packing.

In fact, evaporation occurs along the entire boundary of the droplet, even in the deeper layers of the porous medium. As the conversion from one phase to the other proceeds, the concentration of vapour inside the substrate is increased. If these vapours are not removed, the vapour concentration inside the pores will increase until it reaches saturation levels. Closer to the surface, there is less resistance to vapour migration (or diffusion) to the air stream above. However, in the deeper layers, vapour diffusion is limited by a large layer of the substrate. As a consequence, there is an increase in the vapour concentration in the substrate, which limits the phase change. This behaviour produces a larger evaporation rate in the upper region of the impinged droplet, and less in the deeper layers of the substrate, which physically explains the impression of "drying from the top" as shown by the impinged droplet images.

Another notable feature of the drying process is that after the initial stages of the evaporation, during which the concentration is reduced mainly in the region close to the surface, the liquid concentration is reduced approximately evenly across the full depth of the liquid region. If the local evaporation rates are larger close to the surface, this uniform reduction of concentration across the full depth of the liquid region may indicate that the liquid is migrating from the deeper layers of the substrate to the upper layers, probably due to capillary diffusion. In these circumstances the receding evaporation-front behaviour (assumed in some droplet evaporation models) is not applicable.

It is interesting to note that the images do not display any liquid concentration after $T^* = 0.41$, while the profiles still show a significant amount of liquid in the substrate. In fact, the profiles continue indicating water concentrations until $T^* = 0.46$, as can be observed in Fig. 8a, which presents the mass fraction of liquid remaining inside the substrate based on the integration of the concentration profiles.

At this stage, it is convenient to analyse the time scale of the drying phenomenon. As Fig. 8a shows, the porous substrate (120 μm glass beads) is completely dry at $T^* = 0.46$. This means that the average evaporation rate is in fact nearly two times larger than the value estimated on the basis of the proposed characteristic time scale of the problem (Eq. (3)). One might expect that the drying should be finished with a T^* value larger than 1, due to the limiting effect of the porous medium. However, it must be remembered that the characteristic time scale was estimated based on the evaporation rate of a fully saturated region of liquid with a radius equal to r_0. Thus, the rate of drying in relation to the characteristic time scale is a compromise between the 'slowing down' of the evaporation process caused by the limiting effect of the porous substrate, and the increase in the wetted area exposed to the air stream due to the droplet spread ratio.

Fig. 8b and c show clearly this balance between the two effects. Fig. 8b shows the non-dimensional evaporation rate $(\mathrm{d}M/\mathrm{d}T)^*$ of the droplet, and Fig. 8c shows the non-dimensional mass flux (F^*) to the air stream, which represents the evaporation rate normalised by the area of the wet spot on the substrate. It is possible to observe values of $(\mathrm{d}M/\mathrm{d}T)^*$ well over two, which indicates evaporation rates two times larger than the characteristic evaporation rates. However, the values of F^* are well under 1. This fact indicates that although the evaporation rate is larger than the value for a fully saturated wet spot on the porous substrate, the values per unit area are much smaller. This indicates that there is an increase in the evaporation rate due to the area increase, but there is a significant limiting effect due to the transport mechanism inside the porous medium.

The behaviour described in Fig. 4 for the 120 μm glass beads indicates that the liquid close to the surface dries very quickly, which reflects directly on the drying regimes observed in Fig. 8b. The evaporation rate curve presents a very short, if not negligible, constant-rate period (from $T^* = 0$ to 0.02) and then two distinct falling rates; from this point concentration at the surface starts to fall, as indicated in the profiles shown in Fig. 4, causing the evaporation rate to decrease. However, deeper layers of liquid inside the substrate are still supplying some liquid to the surface, via capillary diffusion, which balances the drying effect. After $T^* = 0.15$ or 0.20 the liquid concentration is reduced approximately evenly across the liquid region, which indicates that there is no longer a sufficient supply of liquid to the surface to support the higher evaporation rate. Thus, the evaporation starts to decrease more rapidly.

3.2. Influence of the porous medium properties

In order to explore the influence of the porous medium properties upon the evaporation process, the size (i.e. diameter) of the glass beads composing the porous

medium was varied. As a consequence, the structure of the porous medium and its porosity is maintained constant, and the permeability and capillary diffusivity are changed. In addition to the variation of glass bead sizes, an additional configuration using sand as the porous substrate was also tested. The rest of the governing parameters were maintained constant.

3.2.1. Shape of the impinged droplet

Fig. 3 presents images of the impinged droplet for 50 μm glass beads (a), 120 μm glass beads (b), 400 μm glass beads (c) and 180 μm sand (d). As outlined in the previous section, the shape of the droplet inside the porous medium is similar to a semi-spheroid, whose aspect ratio will depend on the porous medium and liquid droplet characteristics. The images in Fig. 3 indicate that although the shape resembles a semi-spheroid varying in aspect ratio, there are significant differences between the droplet shapes.

The droplet impinged in 50 μm glass beads shows more irregularities on the upper surface than the other configurations. Since the porous medium is unconsolidated, the particles can be disturbed by the droplet impingement, and (for a given mass density) smaller particles are more easily displaced or dragged by the fluid flow.

Smaller glass beads result in smaller permeability values of the porous substrate, which would restrict the penetration of the liquid, causing it to spread more laterally. Although the observed penetration depth is slightly smaller for 50 μm glass beads than for 120 μm glass beads, the spread ratio is not larger. This discrepancy may be related to the disruption of the upper surface of the shape of the droplet.

On the other hand, there is no disruption of the 400 μm glass beads, since the beads are too large to be displaced by the impact, as indicated by the fact that the upper surface of the impinged droplet appears nearly flat. In this case, the difference in the substrate permeability is sufficient to permit a larger liquid penetration, which yields a smaller lateral spreading. Although the *xz*-slice thickness image resolution is not sufficient to resolve each glass bead, several dark dots are observable and are indicative of the solid glass beads.

By contrast with the droplet impinged on glass beads, the droplet impinged on sand presents a different shape. If the differences were only related to the size of the particles, 180 μm sand should present an intermediate behaviour between 120 and 400 μm glass beads. However, it is likely that there is a considerable difference in the pore structure, shape and size distribution between sand and glass beads, which influence the transport mechanisms inside each substrate, resulting in a larger capillary diffusion effect for sand. This can be clearly observed in the images of the impinged droplet. The droplets impinged in glass beads present a fairly well-defined shape, which indicates a relatively sharp interface. The droplet impinged in sand presents a smoother transition between the saturated region and the dry region, which indicates a significant influence of capillary diffusion. These differences in the porous medium structure also influence the penetration depth of the droplet, which is significantly reduced, yielding a larger lateral spread.

3.2.2. Droplet evaporation

Figs. 4–7 present the time evolution of concentration profiles of liquid and corresponding images of the shape of the droplet inside the porous substrate for each configuration tested, i.e. 120 μm glass beads, 50 μm glass beads, 400 μm glass beads and 180 μm sand.

Fig. 5 shows the results obtained for 50 μm glass beads. In this case, the concentration profile is narrower than the profile for 120 μm glass beads (Fig. 4), since the penetration depth is smaller. As a consequence, the peak concentration value is higher, since the same mass of liquid is distributed over a smaller depth of the porous substrate.

As observed in the base case, the drying starts from the upper surface of the droplet, as can be clearly observed on the concentration profiles by the reduction of the concentration levels in the region close to the surface. However, this reduction occurs much faster than the base case, since the transport of liquid from the deeper layer of liquid is limited by the smaller permeability and capillary diffusivity of the substrate. The profiles and images clearly indicate that there is much more liquid in the deeper layers of the liquid region than on the surface, and it can be seen that there is a receding evaporation-front.

After this initial period, during which the concentration on the surface is reduced, it can be seen that the concentration profiles are reduced homogeneously. At this point the capillary diffusion is strong enough to partially compensate for the evaporation close to the surface, since the evaporation has been significantly reduced.

By contrast with the previous configurations, the 400 μm glass beads substrate does not present a significant reduction in the concentration at the surface (Fig. 6). Although there is a slight change in the shape of the concentration profile throughout the evaporation, this change does not represent a very significant variation in the liquid distribution. This fact can be particularly related to the larger capillary diffusivity of the medium, since the liquid is relatively free to redistribute itself around the region occupied by the droplet.

Fig. 7 presents the concentration profiles and images for the droplet evaporating from 180 μm sand. The initial concentration profile is notably different from the concentration profiles in the previous cases analysed.

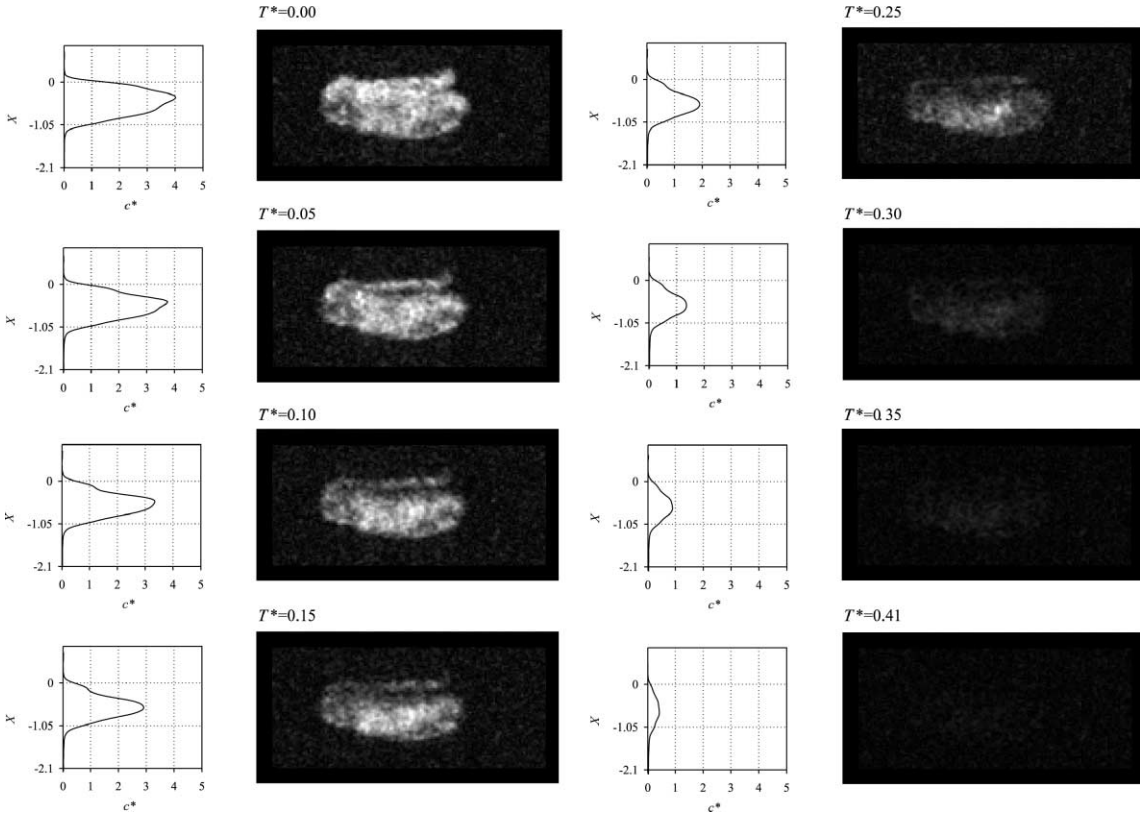

Fig. 5. Time evolution of the water concentration profiles along with the images of the shape of the droplet inside the porous substrate (50 μm glass beads).

The concentration gradients in the lower part of the impinged droplets are much smaller, which characterises a smooth reduction of liquid concentration with depth. As discussed earlier, this fact is mainly related to the increased capillary diffusion effects in sand as compared with glass beads.

As the evaporation proceeds, more liquid is transported by capillary diffusion, and not only does the radius of the impinged droplet increase, but its penetration depth is also increased. Two factors contribute to the reduction of the liquid concentration close to the surface: (i) the evaporation process itself and (ii) the capillary transport into the deeper layers of the substrate.

As a consequence of the increased capillary transport, the droplet evaporation from the sand presents a larger evaporation rate in the initial stages, due to the larger area exposed to the air flow. However, as the evaporation proceeds, liquid migrates deeper into the substrate, severely reducing the evaporation rate. This behaviour can be clearly seen in Fig. 8, which presents the variation of the mass fraction of liquid remaining in the substrate, together with the corresponding values of the evaporation rate of the droplet and mass flux per unit area.

Fig. 8a shows that the mass fraction of liquid remaining in the sand substrate is rapidly reduced in comparison with the glass bead substrates. As time passes the rate of reduction is decreased and the mass fraction of liquid remaining is slowly reduced. This behaviour is even more noticeable in Fig. 8b, where the evaporation rate of the droplet on sand is larger than 3.0, while the values for glass bead substrates are between 2.0 and 2.5. As the evaporation continues, the evaporation rate for sand drops very quickly to values smaller than those of the other configurations, reflecting the effects of the transport of liquid to deeper layers inside the substrate.

Fig. 8c shows that the initial mass flux (evaporation rate per unit area) is approximately similar for all configurations, reflecting the large influence of the spread ratio upon the evaporation rate, and consequently upon the total drying time.

As a general tendency, the characteristics of the porous medium significantly affect the evaporation rate of

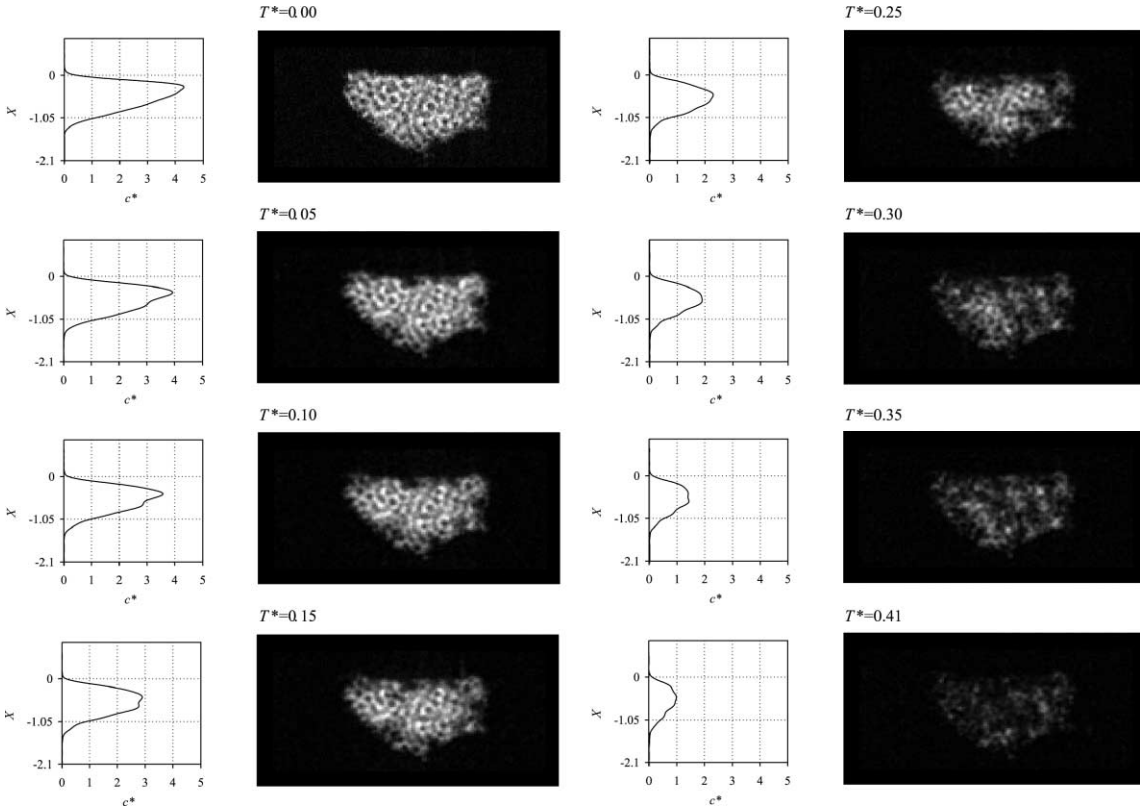

Fig. 6. Time evolution of the water concentration profiles along with the images of the shape of the droplet inside the porous substrate (400 μm glass beads).

the droplets. Although the total evaporation time is approximately similar for all the configurations (in the range from 0.5 to 0.6) the drying regimes are very different.

As discussed in the previous section, the drying curve of the droplet impinged on 120 μm glass beads displays two distinct regions. The first region is characterised by a slow reduction of the liquid concentration close to the surface, when the liquid transport inside the porous medium is still supplying the surface with liquid. In the second region, where the evaporation rate decreases more sharply, the liquid content in the deeper layers of the substrate is no longer sufficient to supply the surface with liquid to sustain the earlier evaporation rate.

This behaviour is not observed on the drying curve of the droplet impinged on 50 μm glass beads, because even in the initial stages of the evaporation the liquid transport is limited by the reduced capillary diffusivity of the substrate. Therefore, the liquid concentration in the surface falls steadily, causing a gradual reduction of the evaporation rate. As a consequence, the droplet takes slightly longer to evaporate.

By contrast, the droplet impinged on 400 μm glass beads presents a drying curve with an initial decrease in the evaporation rate, followed by a marked constant-rate period. The evaporation rate is maintained nearly constant throughout the evaporation episode, due to the constant liquid redistribution inside the substrate (high liquid capillary diffusivity). Accordingly, if this was the only difference in behaviour, the droplet should evaporate completely on a shorter time scale; however, the initial evaporation rate for this configuration is not as high as for the other substrates, due to the reduced spread radius. As a consequence, the total evaporation takes slightly longer than that on 120 μm glass beads.

4. Concluding remarks

Analyses of data from MRI studies on the evaporation of liquid droplets from porous surfaces are presented in this report. The data obtained include images of impinged droplets inside the porous substrate and their variation during evaporation, as well as one-dimensional concentration profiles through the substrates, and time evolution of the mass fraction of liquid remaining and corresponding evaporation rates.

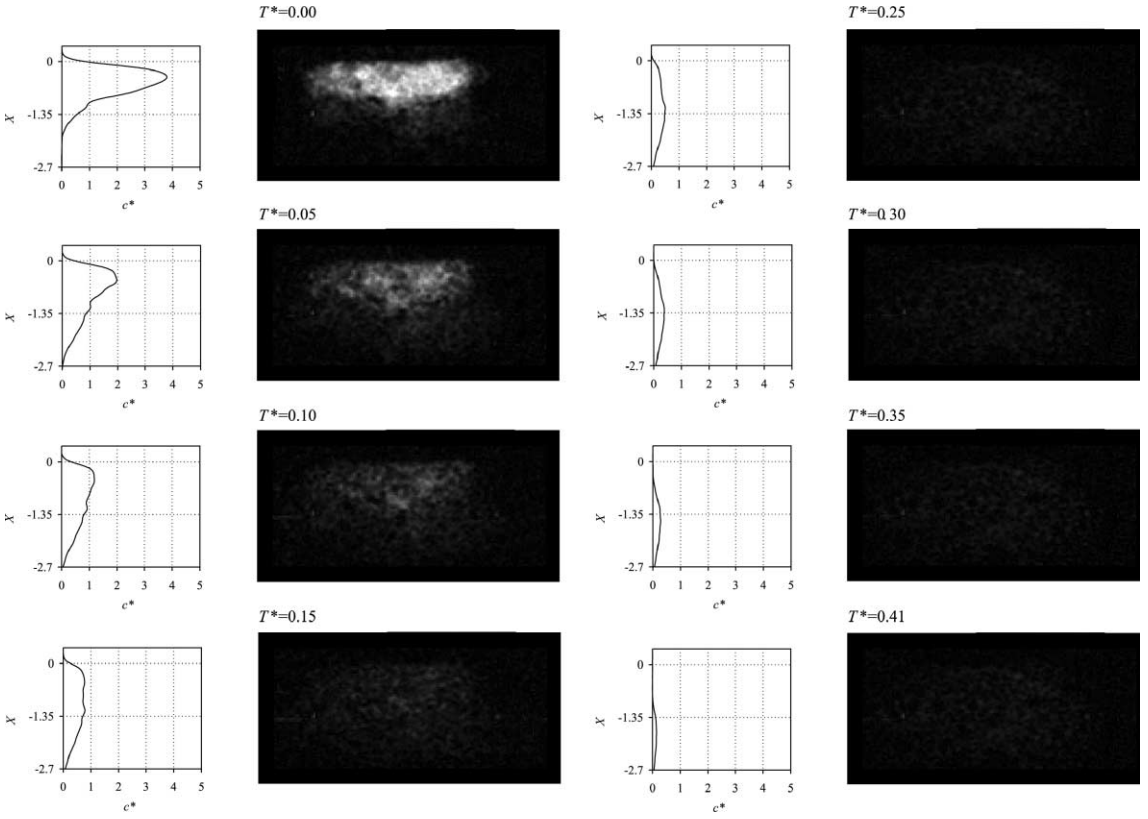

Fig. 7. Time evolution of the water concentration profiles along with the images of the droplet inside the porous substrate (180 μm sand).

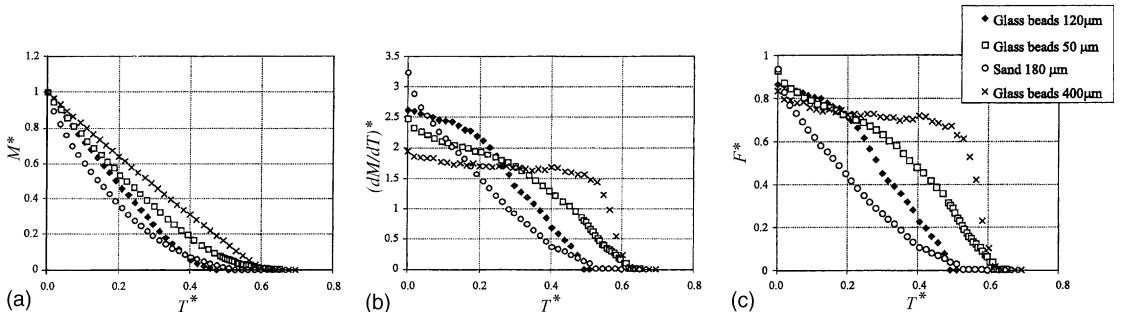

Fig. 8. (a) Mass fraction of liquid remaining inside the substrate based on the integration of the concentration profiles, (b) non-dimensional evaporation rate $(\mathrm{d}M/\mathrm{d}T)^*$ of the droplet vs. T^*, and (c) non-dimensional mass flux (F^*) vs. T^*.

The results obtained show that the impinged droplet resides in the porous medium in a shape similar to a semi-spheroid. The results also indicate that the transport of liquid by capillary diffusion has a very strong influence upon the evaporation process. The data suggest that the liquid embedded in the deeper layers of the substrate continuously supplies the layers close to the surface with liquid, due to capillary diffusion. This indicates that the receding evaporation-front assumption is not appropriate to model the evaporation process in these conditions.

Although the total drying times for the porous media tested (sand 180 μm and glass beads 50, 120, and 400 μm diameter) were approximately similar, the drying regimes were very different. This is related to the different spread radius for droplets impinging on substrates with different

characteristics and to the stronger limiting action of substrates with smaller particles upon the liquid transport. In addition, liquid transport mechanisms are especially important for sand, where capillary diffusion plays a very important role in the evaporation process. In this case, the liquid droplet shows continuous spreading in the substrate throughout the evaporation episode.

The present work has answered many practical questions about the evaporation of liquid droplets from porous surfaces. In particular, it has revealed the shape of the liquid droplet just after impingement and its variation during the evaporation process. It is apparent from this study that there is still a considerable amount of both experimental and theoretical work still required. In particular, it would be desirable to extend the scope of the experimental studies to encompass a wider range of liquid and substrate properties, i.e. liquid viscosity, temperature, wetting properties of liquid solid interface, and to use the results to establish the parameters that characterise the different regimes of transport behaviour in the substrate. This should enable some better definition of the range of conditions in which the receding evaporation-front assumption can be used.

Acknowledgements

The authors wish to acknowledge the sponsorship of the Brazilian Government through CAPES (Fundação Coordenação de Aperfeiçoamento de Pessoal de Nível Superior) and DERA (Defence Evaluation and Research Agency—Porton Down, United Kingdom) under agreement number CU013-0000002229.

References

[1] I.D. Roberts, R.F. Griffiths, A model for the evaporation of droplets from sand, Atmos. Environ. 29 (1995) 1307–1317.
[2] R.F. Griffiths, I.D. Roberts, Droplet evaporation from porous surfaces, model validation from field and wind tunnel experiments for sand and concrete, Atmos. Environ. 33 (1999) 3531–3549.
[3] J.F. Oliver, Initial stages of inkjet drop impaction, spreading, and wetting on paper, TAPPI J. 67 (1984) 90–94.
[4] S. Chandra, Avedisian, Observation of droplet impingement on a ceramic porous surface, Int. J. Heat Mass Transfer 35 (1992) 2377–2388.
[5] J.F. Oliver, L. Agbezuge, K. Woodcock, A diffusion approach for modelling penetration of aqueous liquids into paper, Colloids Surf. A 89 (1994) 213–226.
[6] S.N. Westin, S. Winter, E. Karlsson, A. Hin, F. Oeseburg, On modelling of the evaporation of warfare agents on the ground, J. Hazard. Mater. A 63 (1998) 5–24.
[7] I.D. Roberts, The evaporation of neat/thickened agent simulant droplets from porous surfaces, Final report on agreement no. 2044/013/CDBE, UMIST, 1996.
[8] N.C. Reis, Droplet impingement and evaporation from porous surfaces, Ph.D. Thesis, UMIST, 2000.
[9] J. Hennig, A. Nauerth, H. Friedburg, RARE imaging: a fast imaging method for clinical MR, Magn. Reson. Med. 3 (1986) 823–833.
[10] P.T. Callaghan, Principles of Nuclear Magnetic Resonance Microscopy, Clarendon Press, Oxford, 1991.
[11] E.D. Becker, High Resolution NMR: Theory and Chemical Applications, third ed., Academic Press, London, 2000, pp. 233–235.
[12] B. Wang, W. Yu, A method for evaluation of heat and mass transport properties of moist porous media, Int. J. Heat Mass Transfer 31 (1988) 1005–1009.